FERMILAB-CONF-05-627-E

Tevatron Results

Régis Lefèvre [1]
on behalf of the CDF and DØ Collaborations

Institut de Física d'Altes Energies, Universitat Autònoma de Barcelona,
Edifici Cn. Facultat Ciènces UAB, E-08193 Bellaterra, Spain

Abstract. Recent results obtained by the CDF and DØ experiments at the Tevatron Run II are presented. A first part is dedicated to QCD physics where inclusive jet production, dijet azimuthal decorrelations and jet shapes measurements are reported. Electroweak physics is then discussed relating measurements of the W and Z bosons productions, of the forward-backward charge asymmetry in W production, of the W width and of the top quarks mass. The extensive Run II exploration program is finally approached reporting about searches for neutral supersymmetric Higgs bosons in multijet events and for sbottom quark from gluino decays.

Keywords: Tevatron, CDF, DØ, QCD, Electroweak, Supersymmetry, MSSM, Jet, W, Z, Top, Higgs, Bottom, Gluino, Sbottom, Production, Shape, Asymmetry, Width, Mass, Search
PACS: 13.85.-t, 13.87.-a, 14.65.Ha, 14.70.Fm, 14.80.Cp, 14.80.Ly

INTRODUCTION

In Run II, the Tevatron $p\bar{p}$ collider is operating at a center of mass energy of 1.96 TeV. The 36 bunches of protons and anti-protons collide at two interaction points every 396 ns. The peak luminosity has greatly improved since the beginning on Run II and is now about 10^{32} cm^{-2}s^{-1}. The record integrated luminosity in a week is 20 pb^{-1}. The long term luminosity plan of the Tevatron for Run II is to deliver between 4.4 fb^{-1} (base goal) and 8.5 fb^{-1} (design goal) by the end of 2009.

The CDF [1] and DØ [2] detectors are located at the interaction points. Those two multi-purpose experiments have been highly upgraded for Run II. Both have new Silicon micro-vertex tracker, new tracking system and upgraded muon chambers. CDF also has integrated a new time-of-flight detector and new plug calorimeters. DØ has integrated a new solenoid and new pre-showers. Both experiments have new trigger and data acquisition systems and are taking data with good efficiency, around 85 %. At the time of the conference, each experiment had already collected about 0.7 fb^{-1} on tape.

CDF and DØ has developed a very broad and exciting physics program [3, 4]. Important precision measurements are carried on in order to test and further constrain the Standard Model. New physics beyond the Standard Model are also extensively explored. Some recent results from Run II are presented in the following. They are based on data sets corresponding to integrated luminosities between 72 pb^{-1} and 385 pb^{-1} depending on the analysis.

---

[1] Régis Lefèvre is supported by the EU funding under the RTN contract: HPRN-CT-2002-00292, Probe for New Physics.

QCD PHYSICS

Inclusive jet production

The measurement of the inclusive jet production cross section at the Tevatron provides a stringent test of perturbative QCD (pQCD) predictions over almost nine orders of magnitude. The high p_T tail is sensitive to new physics, it probes distances up to around 10^{-19} m. This measurement can also be used to constrain the Parton Distribution Functions (PDFs) at high x and high Q^2. Thanks to the Tevatron increase of center of mass energy, from 1.8 TeV in Run I to 1.96 TeV in Run II, the jet production rate at high p_T has significantly increased, it has been multiply by a factor five around 600 GeV/c for instance. First Run II measurements have already extended the p_T coverage by about 150 GeV/c compared to Run I. In addition, new jet algorithms are now explored following theoretical prescription suggesting that the cone based algorithm used in Run I is not infrared safe and compromises meaningful comparisons with pQCD calculations.

DØ has measured the inclusive jet production cross section in two regions of jet rapidity, $|y^{jet}| < 0.4$ and $0.4 < |y^{jet}| < 0.8$. Jets were reconstructed using the midpoint algorithm [5]. This iterative seed-based cone algorithm uses midpoints between pair of proto-jets as additional seeds which makes the clusterization procedure infrared safe [6]. The following parameters were used: a cone radius of 0.7 in the $Y-\phi$ space and a merging fraction of 50 %. Results based on 378 pb^{-1} of Run II data are presented in figure 1. The measurements are directly compared to Next-to-Leading-Order (NLO) pQCD calculations computed with NLOJET++ [7] using CTEQ6.1M [8] and MRST2004 [9] PDFs, without any correction for non-perturbative contributions. The renormalization and factorization scales were set to the jet transverse momentum $\mu_R = \mu_F = p_T^{jet}$. The non-perturbative contributions, associated with underlying event and hadronization processes, were investigated using PYTHIA [10] and HERWIG [11]. The two Monte Carlos give consistent results: those contributions were found to be small allowing the direct comparison to NLO calculations presented here to be meaningful within an uncertainty between 10 % for p_T^{jet} lower than 100 GeV/c and 5 % at higher transverse momenta. The measurements agree with the theoretical predictions. Experimental errors are dominated by the uncertainty on the jet energy scale. The largest theoretical error is coming from the PDFs, theoretical predictions especially suffer from the limited knowledge of the gluon distribution at high x.

In CDF, the inclusive jet production cross section has been measured for central jets, $0.1 < |y^{jet}| < 0.7$, using the longitudinally invariant K_T algorithm [12]. Merging pairs of nearby particles in order of increasing relative transverse momentum, as suggested by pQCD gluon emissions, this algorithm is infrared and collinear safe to all orders in pQCD. Unlike cone based algorithms, it does not include any merging/splitting feature that may affect comparisons to pQCD. It contains a parameter D that controls the merging termination and characterizes the approximate size of the resulting jets:

$$d_{ij} = min(p_{T,i}^2, p_{T,j}^2) \cdot \frac{(y_i - y_j)^2 + (\phi_i - \phi_j)^2}{D^2} \; ; \; d_{ii} = p_{T,i}^2$$

To make sure that soft contributions such as the underlying event and multiple $p\bar{p}$

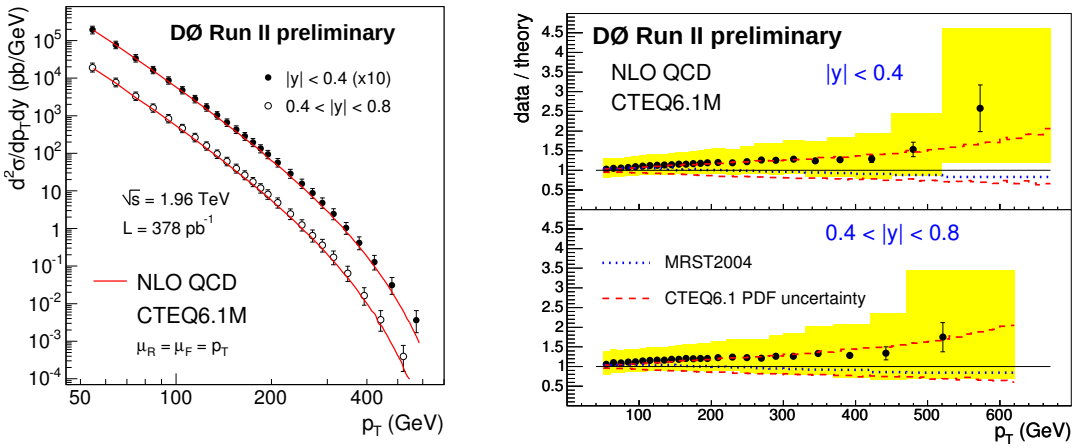

FIGURE 1. *Left:* Inclusive jet cross section measured by DØ in two regions of jet rapidity using the midpoint algorithm. The errors bars indicate the total experimental uncertainty. The data at $|y^{jet}| < 0.4$ are scaled by a factor of ten for presentation purposes. The predictions from NLO pQCD are overlaid on the data. *Right:* Ratio of the measured inclusive jet cross section and the NLO pQCD prediction in the two regions of jet rapidity. The total experimental uncertainty is shown by the shaded bands. The uncertainty due to the proton PDFs is indicated by the dashed lines. The NLO prediction for MRST 2004 PDFs are shown as the dotted line.

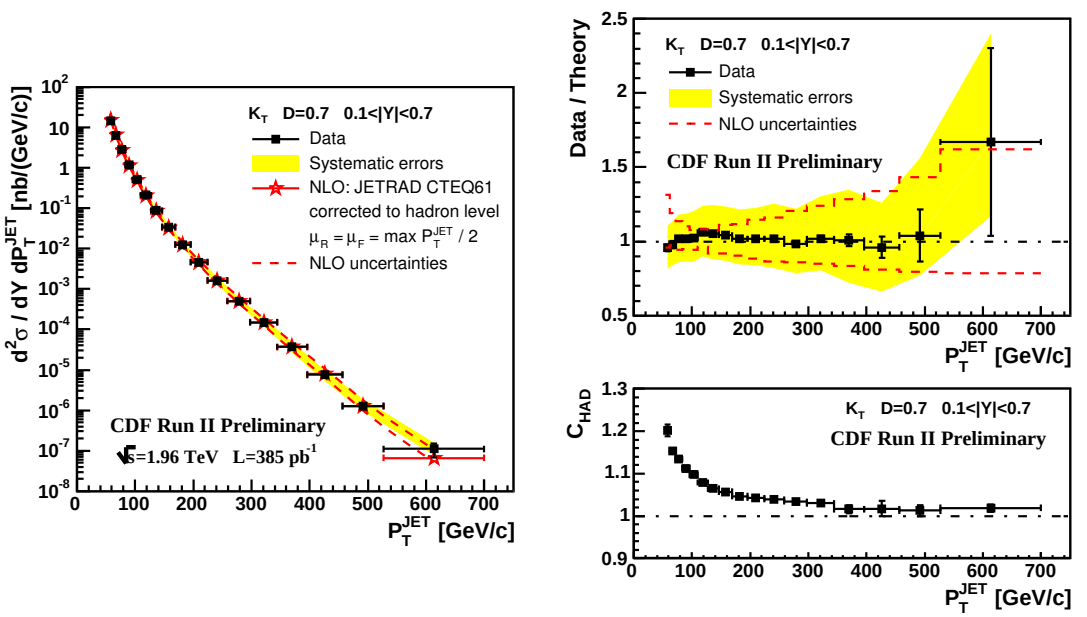

FIGURE 2. Inclusive jet cross section measured by CDF for jets with $0.1 < |y^{jet}| < 0.7$ using the longitudinally invariant K_T algorithm. The measured cross section is compared to NLO pQCD predictions corrected to the particle level: the bottom right plot shows the correction factor that take into account both underlying event and hadronization effects. Data points include the statistical errors, the shaded bands represent the experimental systematic uncertainties. The dashed lines represent the theoretical uncertainties.

interactions are under control, three different values of the D parameter were investigated with 385 pb^{-1} of Run II data: $D = 0.5$, 0.7 and 1.0. The results obtained with $D = 0.7$ are presented in figure 2. They are compared to pQCD NLO predictions computed with JETRAD [13] using CTEQ6.1M PDFs and corrected to the particle level. The renormalization and factorization scales were set to half of the maximum jet transverse momentum in the rapidity region $\mu_R = \mu_F = p_T^{max}/2$. pQCD predictions are corrected to the particle level to take into account the non-perturbative contributions associated with underlying event and hadronization processes, see bottom right plot of figure 2. This correction has been obtained with PYTHIA comparing the predicted jet inclusive cross sections at the particle level with Multiple Parton Interactions (MPI) turned on, and at the parton level with Multiple Parton Interactions turned off:

$$C_{HAD} = \sigma^{PYTHIA-Tune\ A\ with\ MPI\ ON}_{Particle\ level} / \sigma^{PYTHIA-Tune\ A\ with\ MPI\ OFF}_{Parton\ level}$$

for each p_T^{jet} bin. A special set of PYTHIA parameters, tuned on Run I CDF data to reproduce the underlying event activity in the transverse region, denoted as PYTHIA-Tune A [14], was used to evaluate this correction. After correcting pQCD calculations to the particle level, the measurements are in very good agreement with the theoretical predictions over the whole p_T^{jet} range. As for the DØ study previously discussed, systematic errors are dominated by the uncertainty on the jet energy scale while theoretical uncertainties mainly comes from the gluon PDF at high x. Similar very good agreements between data and theory were obtained using a D parameter of 0.5 and of 1.0 showing that soft contributions are well under control as their importance depends a lot on the size of the jets: with respect to $D = 0.7$, the corrections of pQCD to the particle level are for instance about twice smaller using $D = 0.5$ and about twice bigger using $D = 1.0$.

Dijet azimuthal decorrelations

Using an inclusive dijet sample corresponding to 150 pb^{-1} of Run II data, DØ has studied the dijet azimuthal decorrelations measuring the normalized differential dijet cross section in $\Delta\phi_{dijet}$ [15]. This measurement is sensitive to the gluon radiation spectrum.

Jets were reconstructed with the midpoint jet algorithm using a cone radius of 0.7 and a merging fraction of 50 %. Both jets were required to have central rapidities: $|y^{jet}| < 0.5$. Four regions of leading jet transverse momentum were investigated starting at $p_T^{max} > 75$ GeV/c, the second jet was required to have $p_T^{jet} > 40$ GeV/c.

The measurements are reported in figure 3. In the left plot, they are compared to pQCD Leading-Order (LO) and NLO calculations computed with NLOJET++ using CTEQ6.1M PDFs. The renormalization and factorization scales were set to $\mu_R = \mu_F = p_T^{max}/2$. The LO prediction, with at most three partons in the final state, is limited to $\Delta\phi_{dijet} > 2\pi/3$ corresponding to three partons of equal transverse momenta, *Mercedes-star* topology. It presents a prominent peak at $\Delta\phi_{dijet} = \pi$ corresponding to the soft limit for which the third parton is collinear to the direction of the two leading partons. The NLO prediction, up to four partons in the final state, describes the measured distribution except close to $\Delta\phi_{dijet} = \pi$ which is dominated by soft processes

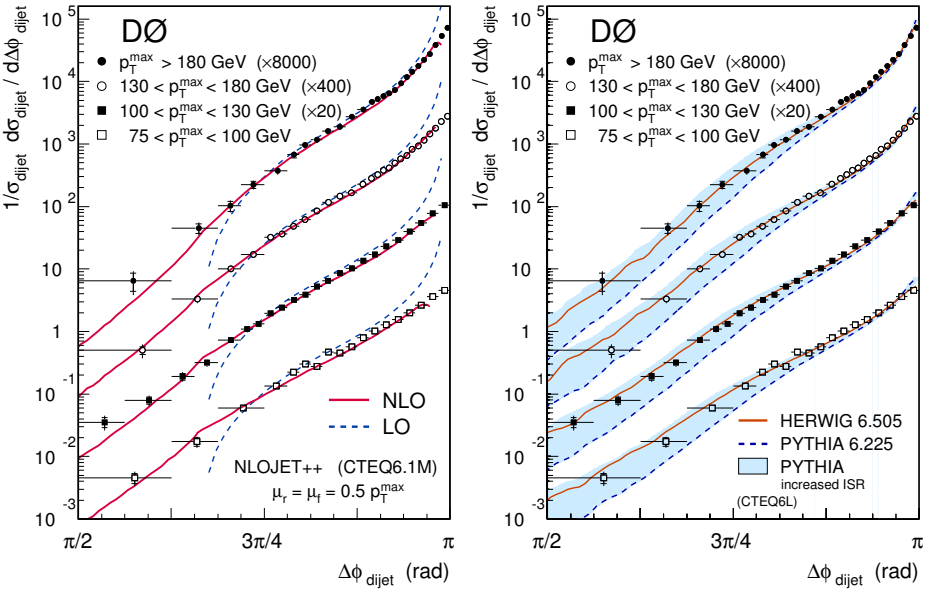

FIGURE 3. $\Delta\phi_{dijet}$ distributions measured in four regions of p_T^{max}. Data and predictions with $p_T^{max} > 100$ GeV/c are scaled by successive factors of 20 for presentation purposes. Predictions are either from NLO (solid lines) and LO pQCD (dashed lines) on the left, either from HERWIG (solid lines) and PYTHIA (dashed lines plus shaded bands, see text) on the right.

and where a resummed calculation is mandatory. A reasonnable approximation to such a calculation is provided by parton shower Monte Carlo programs. In the right plot of figure 3, the measurements are compared to HERWIG and PYTHIA, both with default parameters and CTEQ6L PDFs [8]. HERWIG describes the data. PYTHIA clearly underestimates the gluon radiation at large angles with default parameters but can describes the data if Initial State Radiation (ISR) contributions are increased: the shaded bands in figure 3 (right) indicate the range of variation observed increasing the maximum allowed virtually, directly related to the maximum p_T in the initial-state parton shower, from the default value up to four times higher.

Jet shapes

The internal structure of jets is dominated by multi-gluon emissions from the primary final-state parton. It is sensitive to the relative quark and gluon-jet fraction and receives contributions from soft gluon initial-state radiation and beam-beam remnant interactions. The study of the jet shapes at the Tevatron provides a stringent test of QCD predictions and probes the validity of the models used in the Monte Carlo for parton cascades and soft gluon emissions in $p\bar{p}$ collisions.

Based on an inclusive jet sample corresponding to 170 pb^{-1} of Run II data, CDF has measured the jet shapes for jets with rapidity $0.1 < |y^{jet}| < 0.7$ and transverse momentum $37 < p_T^{jet} < 380$ GeV/c [16]. Jets were reconstructed with the midpoint jet algorithm using a cone radius of 0.7 and a merging fraction of 75 %.

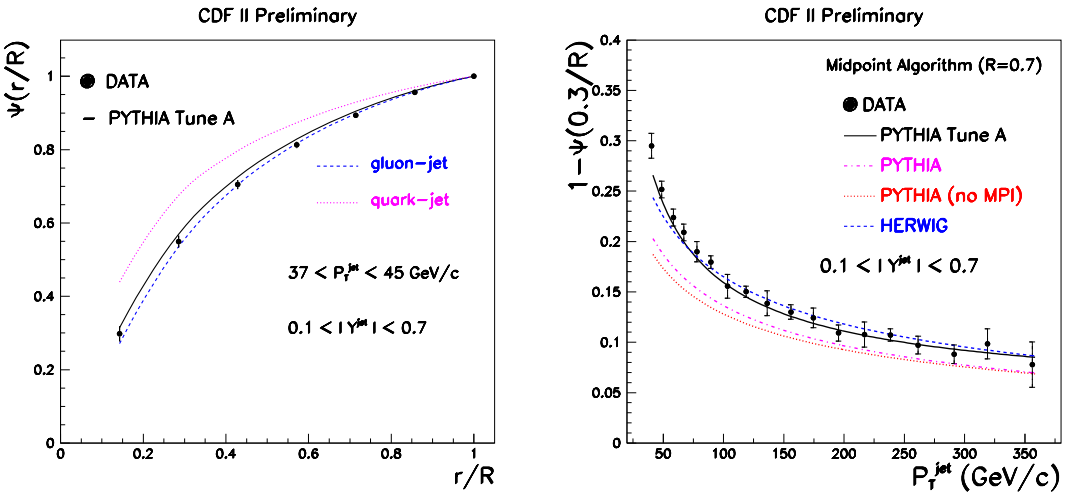

FIGURE 4. *Left:* Measured integrated jet shape for $37 < p_T^{jet} < 45$ GeV/c. The predictions of PYTHIA-Tune A (solid line) and the separate predictions for quark-initiated jets (dotted line) and gluon-initiated jets (dashed line) are shown for comparison. *Right:* $1-\psi(0.3/R)$ versus p_T^{jet}. The predictions of PYTHIA-Tune A (solid line), PYTHIA (dashed-dotted line), PYTHIA-(no MPI) (dotted line) and HERWIG (dashed line) are shown for comparison. In both plots, error bars indicate the statistical and systematic uncertainties added in quadrature.

Figure 4 shows some of the obtained results. The left plot shows the measured integrated jet shape for the first p_T^{jet} bin. It is defined as the average fraction of the jet transverse momentum that lies inside a cone of radius r concentric to the jet cone:

$$\psi(r) = \frac{1}{N_{jet}} \sum_{jets} \frac{p_T(0,r)}{p_T(0,R)}, \quad 0 \leq r \leq R$$

where N_{jet} denotes the number of jets. The right plot of figure 4 shows $1-\psi(0.3/R)$, the average fraction of jet transverse momentum outside an inner cone of fixed radius $r_0 = 0.3$, as a function of p_T^{jet}. The evolution of $1-\psi(0.3/R)$ with p_T^{jet} for gluon-jets only on one hand or for quark-jets only on the other hand is directly related to the running of the strong coupling $\alpha_s(p_t^{jet})$.

The measurements have been compared to the predictions from PYTHIA and HERWIG, using CTEQ5L PDFs [8] in both cases. Tune A parameters were used for PYTHIA, default ones for HERWIG. PYTHIA was also investigated with default parameters and with default parameters but turning off the Multiple Parton Interactions (MPI), the latter solution being denoted as PYTHIA-(no MPI).

With default parameters, PYTHIA produces too narrow jets while PYTHIA-Tune A describes all the data very well. HERWIG gives good predictions for p_T^{jet} above 55 GeV/c but produces too narrow jets bellow. The Monte Carlo predictions indicate that the measured jet shapes are dominated by contributions from gluon-initiated jets at low p_T^{jet} as shown in figure 4 (left), similarly they indicate that contributions from quark-initiated jets dominate at high p_T^{jet}: this is related to the partonic contents of the proton and anti-proton since the quark and gluon mixture in the final state partially reflects the nature on the incoming partons that participate in the hard interaction.

ELECTROWEAK PHYSICS

W and Z productions

In their electron and muon decay modes, the W and Z productions at the Tevatron provide clean, abundant and well know signals that allow stringent tests of the Standard Model. An indirect determination of the W width can for instance be obtained from the ratio of W and Z cross sections. Experimentally more challenging, the tau decay modes are also very interesting as they allow to test the lepton coupling universality.

Figure 5 summarizes the W (left) and Z (right) production measurements that have been performed at the Tevatron. Results are in good agreement with the Standard Model predictions [17]. The main systematic uncertainty arises from the integrated luminosity determination (around 6 %). The second main source of systematic uncertainty comes from the PDFs in the case of the electron and muon decay modes (around 1.5 %). For the tau decay modes, it come from the tau identification (around 5 %).

Making the ratio of the $W \to \mu\nu$ and $W \to e\nu$ cross sections on one hand and the ratio of $W \to \tau\nu$ and $W \to e\nu$ cross sections on the other hand, CDF has investigated the lepton coupling universality to the W boson and found no violation: $g_\mu/g_e = 0.998 \pm 0.004_{(\mathrm{stat})} \pm 0.011_{(\mathrm{syst})}$, $g_\tau/g_e = 0.99 \pm 0.02_{(\mathrm{stat})} \pm 0.04_{(\mathrm{syst})}$.

As there is no sign of non-universality, CDF has made the ratio of the W and Z production cross sections combining electron and muon decay modes and extracted an indirect determination of the W width. The obtained value is $\Gamma_W = 2.079 \pm 0.041$ GeV, compatible with the previous world average $\Gamma_W = 2.124 \pm 0.041$ GeV [18] and in good agreement with the Standard Model expectation $\Gamma_W = 2.092 \pm 0.003$ GeV [18].

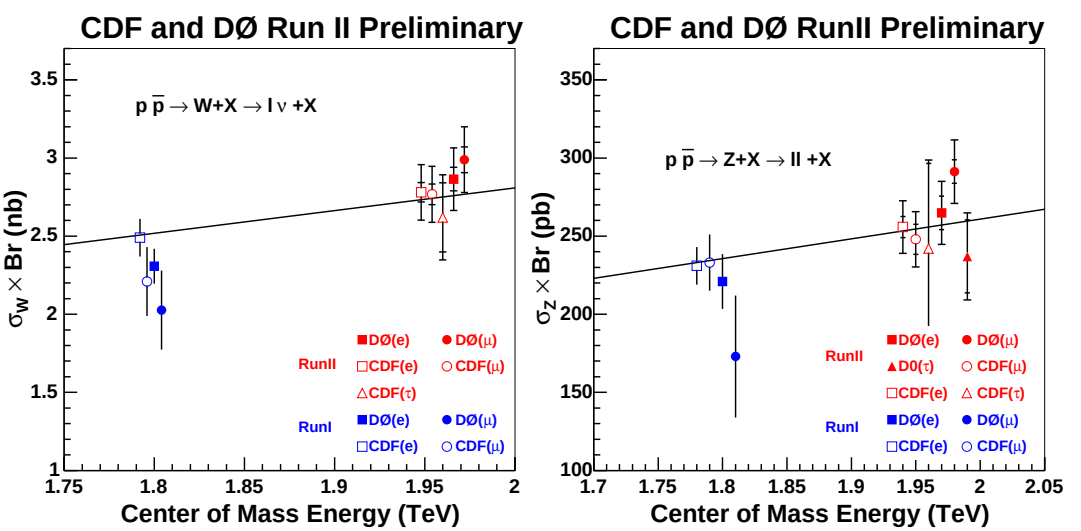

FIGURE 5. Summary of the W (left) and Z (right) production measurements at the Tevatron. Run I (Run II) results are all at 1.8 TeV (1.96 TeV): they are spaced along the x axis for presentation purposes. Inner (outer) error bars on Run II data points exclude (include) the uncertainty from the luminosity measurement. The curves report the Standard Model expectations.

W charge asymmetry

CDF has measured the forward-backward charge asymmetry from $W \to e\nu$ production using 170 pb[1] of Run II data [19]. This measurement provides important input on the ratio of the u and d quark components of the PDFs at high momentum transfer, $Q^2 \approx M_W^2$. Since, on average, u quarks carry a higher fraction of the proton momentum than d quarks [20], produced W^+ (W^-) tend to be boosted forward (backward), in the proton (anti-proton) direction. The $W \to e\nu$ decays provide a high purity sample however, since the p_Z of the neutrino is not reconstructed, the asymmetry can only be measured with respect to the electron pseudo-rapidity , η_e, as:

$$A(\eta_e) = \frac{d\sigma(e^+)/d\eta_e - d\sigma(e^-)/d\eta_e}{d\sigma(e^+)/d\eta_e + d\sigma(e^-)/d\eta_e}$$

As shown in figure 6, the asymmetry has been measured in two intervals of electron transverse energy that probe different ranges of W rapidities and thus increase sensitivity to the PDFs, especially at $x > 0.3$ where they are currently least constrained. Theoretical predictions from CTEQ6.1M [8] and MRST02 [21] PDFs are shown for comparison. They were obtained using NLO RESBOS [22] Monte Carlo calculation with soft gluon resummation to correctly model the p_T spectrum of the W. Inclusion of those results will further constrain future PDFs fits.

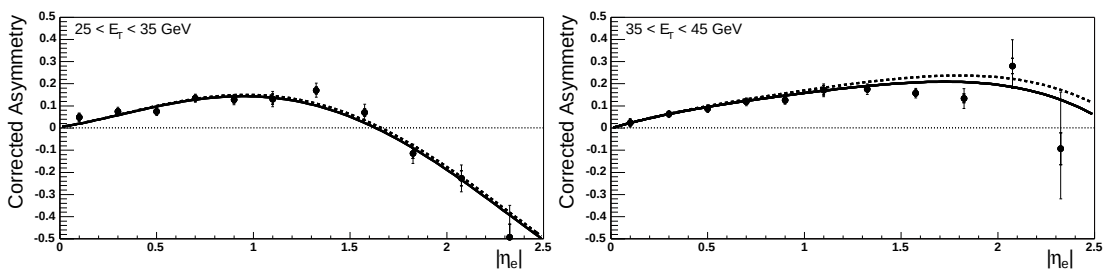

FIGURE 6. Measured forward-backward charge asymmetry from $W \to e\nu$ production as a function of the electron pseudo-rapidity, $A(|\eta_e|)$, for 2 intervals of electron transverse energy: $25 < E_T < 35$ GeV (left) and $35 < E_T < 45$ GeV (right). Theoretical predictions from CTEQ6.1M (solid line) and MRST02 (dashed line) PDFs are overlaid on the data.

Direct measurement of the W width

In the Standard Model, the width of the W boson is precisely predicted in terms of the masses and coupling constants of the gauge bosons: $\Gamma_W = 2.092 \pm 0.003$ GeV [18]. DØ has performed a direct measurement of the W width using 177 pb^{-1} of Run II data in the $W \to e\nu$ channel. It was determined from a binned maximum likelihood fit to the transverse mass distribution in the region $100 < \mathrm{M_T} < 200\ \mathrm{GeV/c^2}$. Figure 7 (left) shows the good agreement between data and Monte Carlo for the fitted width. The obtained result is $\Gamma_W = 2.011 \pm 0.093_{(\mathrm{stat})} \pm 0.099_{(\mathrm{syst})}$ GeV, in good agreement with the Standard

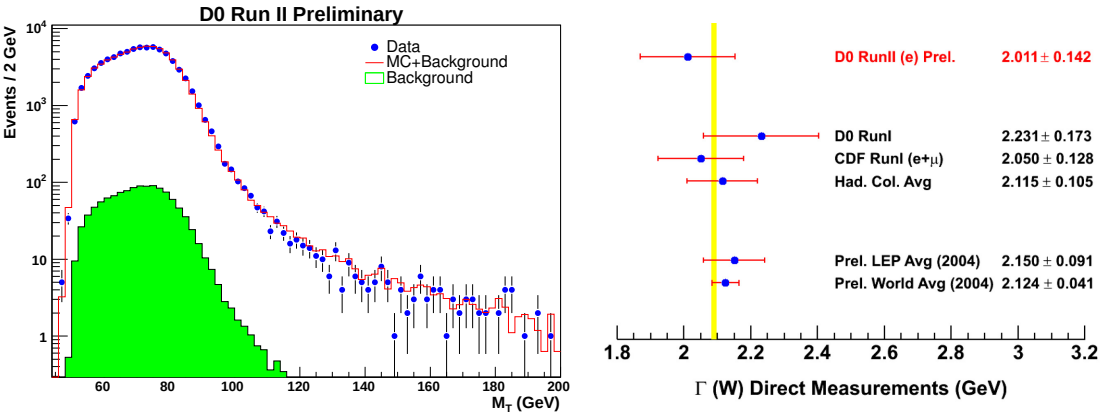

FIGURE 7. *Left:* Comparison of data to Monte Carlo templates for the shape of the transverse mass in $W \to e\nu$ candidates. The dots with error bars are data. The shadowed area is the QCD background. The line corresponds to the sum of the QCD background and of the $W \to e\nu$ and $W \to \tau\nu$ Monte Carlo samples for the fitted value of the W width. The normalization of the Monte Carlo samples is obtained in the transverse mass region $50 \leq M_T \leq 100$ GeV/c^2. The W width is then obtained fitting the tail region $100 \leq M_T \leq 200$ GeV/c^2. *Right:* Comparison of the preliminary result obtained in this analysis to previously published direct measurements of the W boson width. The shaded band indicates the Standard Model prediction.

Model prediction. The main systematic uncertainties come from the modeling of the hadronic response and resolution (64 MeV), the underlying event (47 MeV) and the electromagnetic response (30 MeV). Figure 7 (right) shows that the achieved uncertainty is comparable to Run I ones.

Top quark mass

The top quark mass is a fundamental parameter of the Standard Model. Because radiative corrections are often dominated by the large top quark mass, it plays an important role toward precise prediction of electroweak observables, such as the Higgs boson mass as shown in figure 8 (left). Due to its large mass, the top quark is particularly sensitive to the electroweak symmetry breaking mechanism. A precise measurement of the top quark mass provides a crucial test of the consistency of the Standard Model and help constraining physics beyond the Standard Model.

At the Tevatron, the top quark is mostly pair produced through quark-antiquark annihilation and gluon-gluon fusion. Thanks to the Tevatron increase of center of mass energy, from 1.8 TeV in Run I to 1.96 TeV in Run II, the cross section has increased by about 30 %. Run II experimental results for what concerns the top quark pair production cross section agree with the Standard Model expectation [23].

Because its width ($\Gamma_t > 1$ GeV for $m_t > 120$ GeV/c^2) is quite larger than Λ_{QCD} (≈ 100 MeV), the top quark decays before hadronizing. In the Standard Model, the top quark decays almost exclusively to a W boson and a b quark. $t\bar{t}$ events are then classified with respect to the W decays. The most precise measurements of the top quark mass are

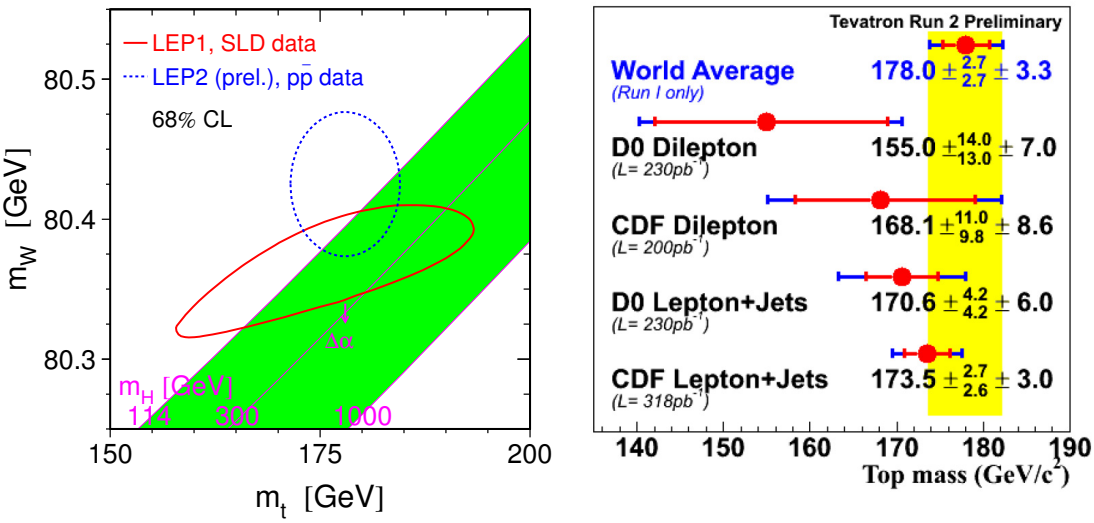

FIGURE 8. *Left:* Mass of the Higgs boson predicted by the electroweak fit as a function of the top quark mass and the W boson mass. Direct and indirect experimental contraints are also reported, they do not include Run II preliminary results. *Right:* Best Run II preliminary measurements of the top quark mass. The shaded band represents the world average from Run I.

obtained in the lepton plus jets sample in which one of the W decays to leptons and the other to quarks. The measurement has also been performed in the dilepton sample in which both W decay to leptons.

Figure 8 (right) summarizes the best Run II preliminary results at the time of the conference. CDF lepton plus jets analysis is the most recent one and achieves the best precision, even better than previous world average from Run I. In this study, the observed invariant mass distribution of the W hadronic decays is used to reduce the largest systematic uncertainty which arises from the jet energy scale. The different measurements agree with Run I combination, the central values tend to be a bit smaller.

SEARCHES

Search for neutral supersymmetric Higgs in multijet events

DØ has searched for neutral supersymmetric Higgs bosons produced in association with bottom quarks using 260 pb^{-1} of data collected in Run II. In the Minimal Supersymmetric extension of the Standard Model (MSSM), the $bb\phi(\rightarrow bb)$ processes are enhanced at large tan β. An excess in the distribution of the two leading jets invariant mass in events with at least three b-tagged jets was investigated.

Figure 9 (left) shows that the obtained dijet mass spectrum agrees very well with the estimated background. Limits on signal production cross sections were then set using a modified frequentist method [24]. Expected signal cross sections in the MSSM and their uncertainties were taken from NLO calculations [25, 26]. Figure 9 (right) shows the obtained limits in the tan β versus m_A plane on two MSSM scenarios: “no mixing”

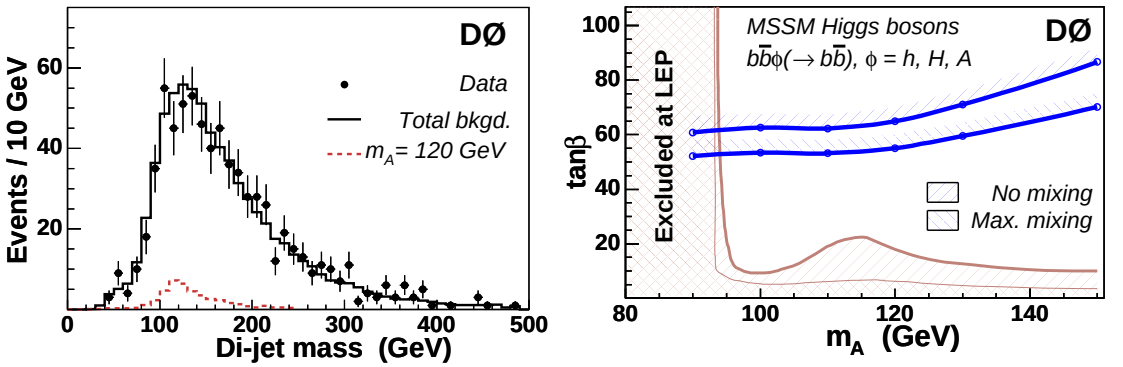

FIGURE 9. *Left:* Invariant mass spectrum of the two leading jets in events with at least three b-tagged jets, estimated background and expected signal for a 120 GeV/c^2 Higgs boson that can be excluded at 95 % CL. *Right:* 95 % CL upper limit on tan β as a function of m_A for the two scenarios of the MSSM, "no mixing" and "maximal mixing". Also shown are the limits obtained by the LEP experiments for the same two scenarios of the MSSM.

in the scalar top quark sector [27, 28], $X_t = A_t - \mu \cot\beta = 0$ where A_t is the tri-linear coupling and $\mu = -0.2$ TeV in the Higgsino mass parameter, and "maximal mixing", $X_t = \sqrt{6} \times M_{SUSY}$ where $M_{SUSY} = 1$ TeV is the mass scale of supersymmetric particles. A significant portion of the parameter space is excluded down to tan $\beta \approx 50$.

Search for sbottom quarks from gluino decays

CDF has searched for sbottom quarks from gluino decays using 156 pb^{-1} of Run II data. For supersymmetric scenarios with large tan β, the lighter sbottom mass eigenstate ($\tilde{b}_1$) can be significantly lighter than other squarks due to the substantial mixing in the sbottom sector [29]. This analysis assumes a scenario where the sbottom quark is lighter than the gluino and relies on the large gluino pair production cross section. R-parity conservation is assumed and the Lighest Supersymmetric Particle (LSP) is supposed to be the lighest neutralino ($\tilde{\chi}_1^0$). Each of the pair produced gluinos decays as follow: $\tilde{g} \rightarrow b\tilde{b}_1 \rightarrow b\bar{b}\tilde{\chi}_1^0$. The analysis requires four jets, large missing E_T and one or two b-tagged jets. In the more sensitive inclusive double b-tagged sample, see figure 10 (left), 4 events were observed in the signal region, missing $E_T > 80$ GeV, where 2.6 ± 0.7 events were expected from Standard Model processes. Figure 10 (right) shows the obtained limits in the gluino sbottom mass plane. Earlier limits are significantly extended.

ACKNOWLEDGMENTS

I am very grateful to the DIS 2005 organizers for their invitation. I would also like to acknowledge the members the CDF and DØ Collaborations for their works in achieving the results reported here. Finally, I would like to acknowledge the EU for its funding under the RTN contract: HPRN-CT-2002-00292, Probe for New Physics.

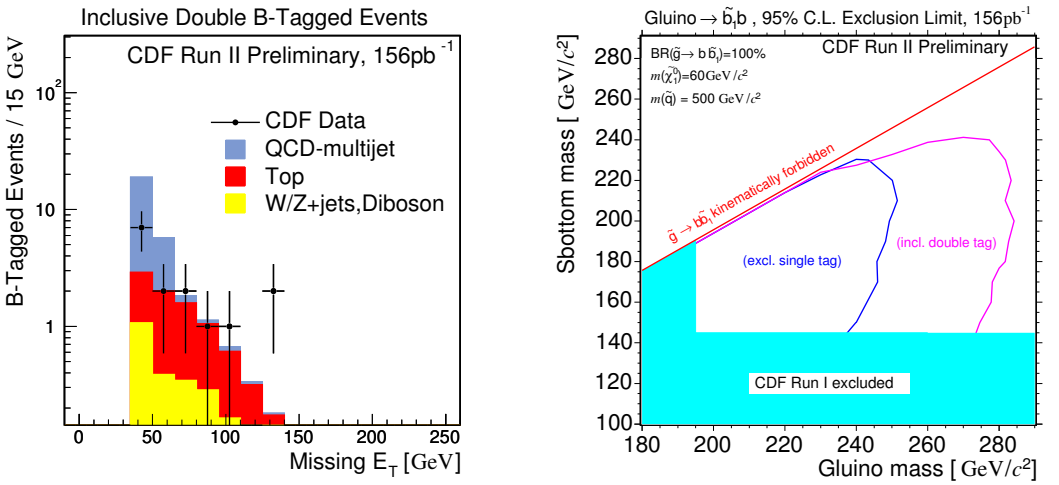

FIGURE 10. *Left:* missing E_T spectrum in the inclusive double b-tagged sample. Estimated backgrounds are overlaid on the data. *Right:* 95 % CL exclusion contours in the gluino sbottom mass plane obtained in the exclusive single b-tagged sample and in the inclusive double b-tagged sample. Previous limits from Run I are also reported.

REFERENCES

1. CDF Collaboration, D. Acosta *et al.*, Phys. Rev. D **71**, 032001 (2005).
2. T. LeCompte and H.T. Diehl, Annu. Rev. Nucl. Part. Sci. **50**, 71 (2000).
3. CDF Collaboration, http://www-cdf.fnal.gov/physics/physics.html
4. DØ Collaboration, http://www-d0.fnal.gov/Run2Physics/WWW/results.htm
5. G.C. Blazey *et al.*, Proceedings of the Workshop: "QCD and Weak Boson Physics in Run II", Batavia, Illinois, 1999, edited by U. Baur, R.K. Ellis and D. Zeppenfeld, 47 (2000).
6. M.H. Seymour, Nucl. Phys. B **513**, 269 (1998).
7. Z. Nagy, Phys. Rev. Lett. **88**, 122003 (2002); Z. Nagy, Phys. Rev. D **68**, 094002 (2003).
8. J. Pumplim *et al.*, JHEP **0207**, 12 (2002); D. Stump *et al.*, JHEP **0310**, 046 (2003).
9. A.D. Martin *et al.*, Phys. Lett. B **604**, 61 (2004).
10. T. Sjöstrand *et al.*, Comp. Phys. Comm. **135**, 238 (2001).
11. G. Marchenisi *et al.*, Comp. Phys. Comm. **65**, 465 (1992); G. Corcella *et al.*, JHEP **0101**, 010 (2001).
12. S.D. Ellis and D.E. Soper, Phys. Rev. D **48**, 3160 (1993).
13. W.T. Giele *et al.*, Phys. Rev. Lett. **73**, 2019 (1994).
14. R.D. Field, "ME/MC Tuning Workshop", Fermilab, October 2002.
15. DØ Collaboration, V.M. Abazov *et al.*, Phys. Rev. Lett. **94**, 221801 (2005).
16. CDF Collaboration, D. Acosta *et al.*, FERMILAB-PUB-05-156-E, accepted by Phys. Rev. D (2005).
17. C.R. Hamberg, W.L. van Neerven and T. Matsuura, Nucl. Phys. B **359**, 343 (1991).
18. S. Eidelman *et al.*, Phys. Lett. B **592**, 1 (2004).
19. CDF Collaboration, D. Acosta *et al.*, Phys.Rev. D **71**, 051104 (2005).
20. H.L. Lai *et al.*, Phys.Rev. D **51**, 4763 (1995).
21. A. Martin, R. Roberts, W. Stirling, and R. Thorne, Eur. Phys. J. C **4**, 463 (1998).
22. F. Landry, R. Brock, P. M. Nadolsky, C. P. Yuan, Phys. Rev. D **67**, 073016 (2003).
23. M. Cacciari *et al.*, JHEP **404**, 068 (2004).
24. T. Junk, Nucl. Instrum. Methods Phys. Res. A **434**, 435 (1999).
25. J. Campbell, R.K. Ellis, F. Maltoni and S. Willenbrock, Phys. Rev. D **67**, 095002 (2003).
26. S. Dawson, C.B. Jackson, L. Reina and D. Wackeroth, Phys. Rev. Lett. **94**, 031802 (2005).
27. M. Carena, S. Mrenna and C.E.M. Wagner, Phys. Rev. D **60**, 075010 (1999).
28. M. Carena, S. Mrenna and C.E.M. Wagner, Phys. Rev. D **62**, 055008 (2000).
29. A. Bartl, W. Majerotto ans W. Porod, Z. Phys. C **64**, 499 (1994); Erratum-ibid. C **68**, 518 (1995).